Teng et al. *EPJ Quantum Technology* (2023) 10:33
https://doi.org/10.1140/epjqt/s40507-023-00189-8

EPJ Quantum Technology
a SpringerOpen Journal

RESEARCH Open Access

# Arbitrary bias control of $LiNbO_3$ based Mach-Zehnder intensity modulators for QKD system

Jun Teng[1,2], Shuang Wang[1,2,3*], Zhen-Qiang Yin[1,2,3], Wei Chen[1,2,3], Guan-Jie Fan-Yuan[1,2], Guang-Can Guo[1,2,3] and Zheng-Fu Han[1,2,3]

*Correspondence:
wshuang@ustc.edu.cn
[1]CAS Key Laboratory of Quantum Information, University of Science and Technology of China, Hefei 230026, P.R. China
[2]CAS Center for Excellence in Quantum Information and Quantum Physics, University of Science and Technology of China, Hefei 230026, P.R. China
Full list of author information is available at the end of the article

**Abstract**

Quantum key distribution (QKD) can help distant agents to share unconditional secret keys, and the achievable secret key rate can be enhanced with the help of decoy-state protocol. To implement QKD experimentally, the agents are supposed to accurately transmit a number of different intensity pulses with the $LiNbO_3$ based Mach-Zehnder (LNMZ) intensity modulator. However, the bias drift of LNMZ intensity modulator may affect the performance of a QKD system. In this letter, we reveal a simple RC circuit model to demonstrate the bias drift in the LNMZ intensity modulator. And based on the model, we propose a multi-step bias stable scheme to control the bias working point. Experimental result shows that our scheme can eliminate the bias drift of at arbitrary working point within a long time range. Besides, there is no need of any feedback mechanisms in the scheme. This means our scheme will not lead to any increasement in system complexity, making it more suitable for a QKD system.

## 1 Introduction

Quantum key distribution (QKD) allows two distant agents (Alice and Bob) to share unconditional secret keys [1–14], and the security of it is guaranteed by quantum physics with the assumption that the key is transmitted with single photons. However, an ideal single-photon source that is suitable for QKD is still not yet available in experiments, despite the significant development of single-photon production. Thus we usually choose the weak coherent pulses as an alternative resolution. With the help of decoy-state method [15–17], the QKD schemes using weak coherent pulses can perform competitive key rates as those using the ideal single-photon.

The idea behind decoy-state method is quite straightforward, users varies the mean photon number of each pulse to estimate the behavior of the quantum channel, this helps to enhance the achievable secret key rates and communicating distance. To perform decoy-state method experimentally, a $LiNbO_3$ based Mach-Zehnder (LNMZ) intensity modulators are usually used here. However, one of the largest concerns during the development of $LiNbO_3$ technology is the issue of bias drift [18–21], which is critical for the performance

of LNMZ intensity modulators. For example, in the QKD systems, the light intensities should be accurately modulated. Otherwise, if there is a bias drift in the modulator, which leads to an intensity fluctuation of the pulses, the secure key rates of QKD may drop rapidly and the QKD system may suffer from side channels.

Several reasons can lead to the bias drift in an LNMZ modulator. The extrinsic sources, for example, are due to changes of environmental conditions including temperature, humidity or stress [22–25]. The intrinsic origin is related to the flow and redistribution of electrical charge in the device structure under the application of voltage. In order to optimize the modulation signal, such as accurately modulating the light intensities in QKD systems, it is essential to lock the bias working point, to ensure that the modulator can work at a suitable point in the transfer function curve. It is reported that the extrinsic source is not the dominant reason for bias drift [26], and several techniques for reducing the effect of these extrinsic sources of bias drift are known, while the intrinsic was not widely investigated. There are primarily two types of MZM bias control methods: one that utilizes optical power monitor and the other that utilizes a dither signal. In the former case [27–29], the input and output power or their ratio are used as the feedback signal. In the latter case [30–32], a dithering signal is used to generate the first- and second-order harmonics, and, subsequently, the bias voltage is controlled according to their power ratio. However, neither of these two types is suitable methods for a QKD system. On the one side, both type need external optical feedback modules, which will increase the complexity of the QKD system. On the other side, a dithering signal may induce crosstalk noise, which will affect the performance of QKD system and even lead to potential loopholes.

In this letter, we propose a multi-step bias modulation scheme based on a simplified RC circuit model, The scheme predicts the bias drift on the LNMZ modulators without adding any additional feedback devices, thus it will not increase the system complexity and can be more efficient for QKD systems. The detailed comparisons between our scheme and existing method will be given in Sect. 3.

## 2 The intrinsic DC drift and RC circuit model

The intrinsic DC drift, as reported, originates from the inhomogeneous electrical properties and the electrically anisotropic in $LiNbO_3$ substrate layer [26]. The schematic view of a z-cut LNMZ modulator is shown in Fig. 1. The modulator is mainly composed of electrodes, $SiO_2$ buffer layer, $LiNbO_3$ substrate layer and titanium-diffused waveguides. When a bias voltage is applied between the + and − electrodes, the evolution of the electric field in the modulator can be described as follow:

$$\begin{cases} \mathrm{div}([\epsilon]\vec{\boldsymbol{E}}) = \rho, \\ \mathrm{div}([\theta]\vec{\boldsymbol{E}}) = -\frac{\partial \rho}{\partial t}, \end{cases} \tag{1}$$

where $[\epsilon]$ and $[\theta]$ are the dielectric permittivity and electrical conductivity tensors, $\rho$ is the electrical charge density. From Eq. (1) we can know that either of the dielectric permittivity or the electrical conductivity or the applied electric field are inhomogeneous leads to a time-dependent electrical charges redistribution inside the structure of the modulator, inducing a drift of the operating point of the LNMZ modulator.

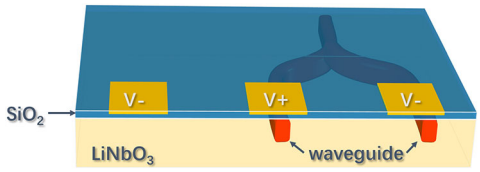


**Figure 1** Schematic view of a z-cut $LiNbO_3$ MZ modulator

In order to numerically analyze the drift in the modulator, we use a normalized drift function $S(t)$ to indicate the value of the drift magnitude.

$$S(t) = \frac{V_m(t) - V_m(0)}{V_m(0)}, \tag{2}$$

where $V_m$ is the phase voltage applied on the waveguide region. Thus $V_m(0)$ is the voltage applied by the electrodes and $\Delta V = V_m(t) - V_m(0)$ is the bias drift. For simplicity, we denote $V_{\text{bias}} = V_m(0)$ as bias voltage, $\Delta V$ as drift voltage and $V_m(t)$ as the phase voltage.

To facilitate process on the understanding and engineering of the bias stability of the component, several RC models have been proposed [26, 33–35]. Yamada and Minakata discussed charge storage in oxide buffer layers using very simple circuits [33], whereas Becker [34] was focused only on the role of the built-in electrical anisotropy of the $LiNbO_3$ substrate. In Ref. [26], the RC model considered both buffer layer and the anisotropy of the $LiNbO_3$ substrate.

In Ref. [35], the authors proposed a general RC circuit model and derived the time domain solution for the case of an arbitrary number of material layers. In this model, the buffer layer, substrate, and waveguide region of the substrate were all taken into account. In the network model, each of the the materials in the LNMZ modulator is characterized by its permittivity and conductivity. Thereafter, an simplified equivalent RC ladder network can be proposed. An general solution to the RC network consisting of N ladder sections can be expressed as follow:

$$V_i(t) = V_e(0)\left(a_{i0} + \sum_{j=1}^{N} a_{ij} e^{-t/\sigma_j}\right), \tag{3}$$

where the $i$th ladder section is defined to consist of the combination of the $i$th parallel and series RC pair, and $V_i(t)$ is the voltage drop across the $i$th parallel RC pair, and it is easy to know that $V_1(t)$ is the phase voltage $V_m(t)$ that defined in Eq. (2). The $N$ time-constants $\sigma_j$ are the reciprocals of the short-circuit natural frequencies of the network and the $a_{ij}$ are the constants of the integration.

With the general solution derived above, we are supposed to predict the drift of phase voltage $V_m(t)$ defined in Eq. (2). However, the solution of Eq. (3) is so complicated when the parameter $N$ is large that only numerical calculation is practical. While in experiments, we find that the prediction of $S(t)$ is precise enough when the $N$ is chosen as a small value (two to four is enough). This fact means that a RC network model with only a few RC circuit ladder section is good enough to indicate the bias drift in the LNMZ modulator. In this case, we focus on the simplified RC circuit network model which consists of only

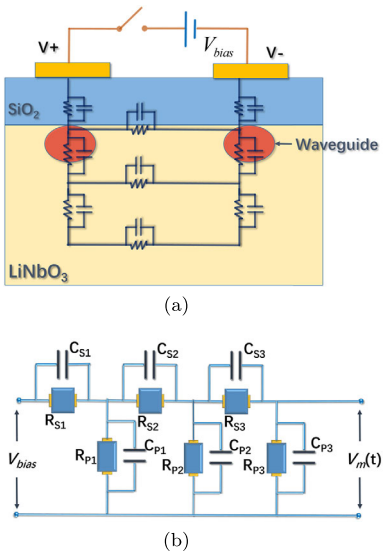


**Figure 2** (a) Equivalent RC circuit that models the time-dependent electrical charges redistribution inside the z-cut LNMZ intensity modulator. (b) The simplified equivalent circuit

three ladder sections. With this simplification, the function in Eq. (3) can be simplified, so that the phase voltage $V_m(t)$ on the waveguide region can be expressed as follow:

$$V_m(t) = V_e(0)\left(a_0 + \sum_{j=1}^{3} a_j e^{-t/\sigma_j}\right), \tag{4}$$

and with the definition in Eq. (2), the drift function of the RC circuit network model can be expressed as follow:

$$S(t) = Ae^{-t/\sigma_1} + Be^{-t/\sigma_2} + Ce^{-t/\sigma_3} + D, \tag{5}$$

where the time constants $A = a_1/a_0 + a_1 + a_2 + a_3$, $B = a_2/a_0 + a_1 + a_2 + a_3$, $C = a_3/a_0 + a_1 + a_2 + a_3$, $D = a_1 + a_2 + a_3/a_0 + a_1 + a_2 + a_3$.

Furthermore, with the simplified network model, a cross-sectional view of the modulator is shown in Fig. 2. Similar to the analyses in Ref. [26], Here we mainly consider the anisotropic $LiNbO_3$ substrate and electrical conductivity modification on the waveguide region where Ti in-diffusion process are applied. Besides, we also take into account the electrical inhomogeneous of the buffer layer. The equivalent RC circuit is presented in Fig. 2(b)

To verify the universality of the model in Eq. (5), we measured the bias drift on a LNMZ modulator of three different initial bias voltages, which corresponds to the peak, trough and quadrature working point of the voltage response curve. As shown in Fig. 4(a), the voltages accordingly are respectively 3.609, 6.007 and 8.405 V.

The experimental arrangement is shown in Fig. 3. The modulator is placed in a temperature controlled ($\pm 0.01$) chamber. The light is delivered by a continuous-wave fiber laser emitting at 1.55 μm wavelength, and is splitted by a 50:50 polarization maintaining beam splitter (BS). One output of the BS is fed into the LNMZ intensity modulator before detected by the optical power monitor, the other output is connected with the optical power monitor directly. In this way, we can pick out the drift of the LNMZ modulator from that

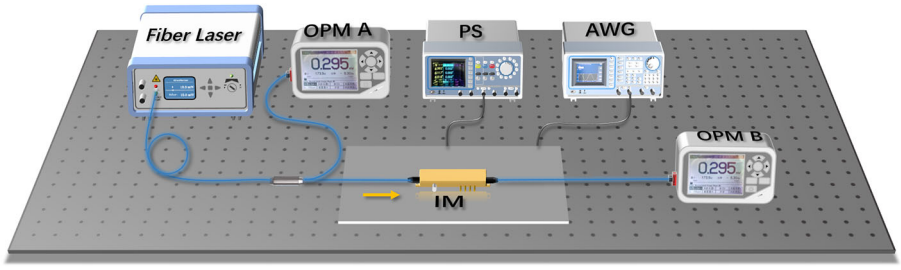


**Figure 3** Schematic of dc drift recording arrangements. IM, the LNMZ intensity modulator; AWG, arbitrary waveform generator; PS, power supply; OPM, optical power monitor

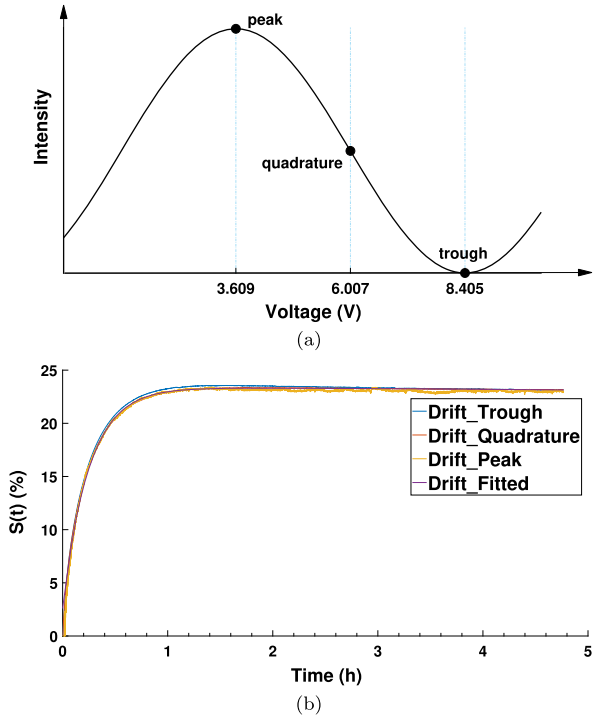


**Figure 4** Experimental dc bias drift of three differing initial bias voltages: (a) the values of three initial bias voltages. (b) normalized bias drift magnitude S(t)

of the laser because the environment may induce a drift on the laser. Besides a bias voltage, the modulator is driven by an ac 10 MHz signal with $V_{p-p}$ = 1.4 V to simply imitate a two decoy scheme in QKD system.

As shown in Fig. 4(b), The drift magnitude $S(t)$ of the three different initial bias voltages over time is presented. And the result shows that the drifts are virtually identical to each other. We add a fitted curve based on the model in Eq. (5), it shows that the curve fits well to the measured drift magnitude. This confirms that the model based on RC circuits is a valid representation of the DC bias drift phenomenon.

## 3 The bias stable scheme

Based on the RC circuits model in Eq. (5), we propose a working point stable scheme, which can control the working point of the LNMZ modulator. In the scheme, we adjust the

input $V_{\text{bias}}$ over time to keep the phase voltage $V_m(t)$ stable. The idea behind is that, in an RC circuit model, when bias voltage applied on the modulator varies, the resulted DC bias drift can be treated as linear superposition of all the previous bias voltage modulations. So that we can predict the bias drift after $n$ th bias voltage modulation. The drift magnitude can be expressed as follow:

$$P_n(t) = \begin{cases} F[V_1(1+S(t))] \quad (0 \le t \le t_1), \\ F[V_1(1+S(t)) + (V_2 - V_1)(1+S(t-t_1))] \quad (t_1 \le t \le t_2), \\ \cdots \\ F[V_1(1+S(t)) + \cdots + (V_n - V_{n-1})(1+S(t-t_{n-1}))] \quad (t_{n-1} \le t \le t_n), \end{cases} \tag{6}$$

where $F(V)$ is the transfer function of the modulator shown in Fig. 4(a). It reveals the relation between voltage applied on waveguide and the output intensity. $V_n$ is the $n$ th bias voltage added to the modulator, and $S(t)$ is the drift magnitude in Eq. (2). $V^n_{\text{phase}} = V_1(1+S(t)) + \cdots + (V_n - V_{n-1})(1+S(t-t_{n-1}))$ is the phase voltage.

To verify the model presented in Eq. (6), we first implemented a simple scheme with two step bias voltage modulation. In the first step, a bias voltage $V_1$ is applied to the modulator, that is $V_m(0) = V_1$, where $V_m(0)$ is defined in Eq. (2). And $V_1$ induced a bias drift $V^1_{\text{drift}}(t)$, which means $V_m(t) = V_1 + V^1_{\text{drift}}$ changes over time, $V_m(t)$ is the phase voltage as defined in Eq. (2). When $V_m(t)$ reaches the value $V_m(t) = 6.007$ V (As shown in Fig. 4(a), 6.007 V corresponds to the quadrature point of the modulator), we applied the second step, in which $V_1$ is modulated to $V_2$, and $V_2 = 6.007$ V. This means $V_m(0)$ is switched from $V_m(0) = V_1$ to the quadrature working point at 6.007 V. The modulation of $V_m(0)$ from $V_1$ to $V_2$ induced another bias drift $V^2_{\text{drift}}(t)$. According to the model in Eq. (6), now the total bias drift on the modulator is the linear superposition of $V^1_{\text{drift}}(t)$ and $V^2_{\text{drift}}(t)$. Our experimental result is shown in Fig. 5, it shows the result fits the model in Eq. (6) well. This means our model is feasible in this two step modulation scheme.

In the simple two step scheme above, we experimentally verified that our model in Eq. (6) can predict the output power after a simple two step modulation on the LNMZ modulator. Naturally, we then implemented a multi-step scheme. In the multi-step scheme, an original bias voltage is applied to set the modulator to its working point, here the working point we choose is the quadrature point. Then the bias voltage is continuously adjusted to maintain the working point. From model in Eq. (6), we can find that maintaining the bias working

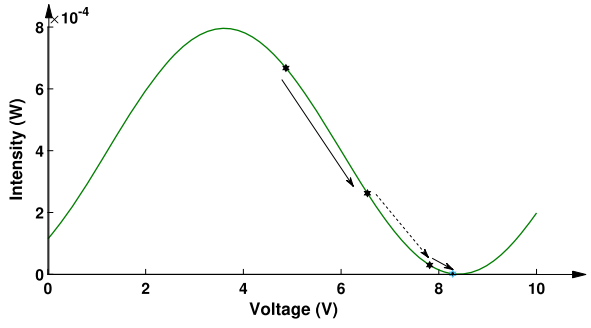


**Figure 5** Experimental two step test of the bias stable scheme

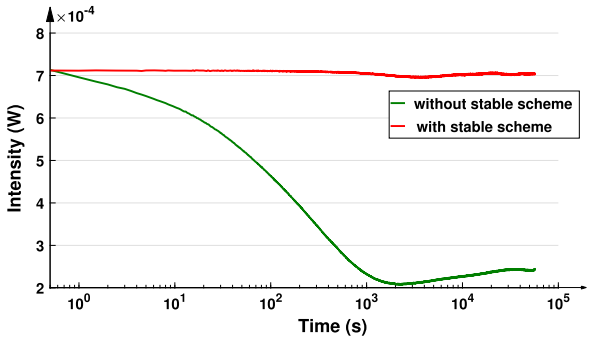


**Figure 6** Experimental multi-step test of the bias stable scheme. The drift magnitude with multi-step stable scheme is 1.61 % of that without one

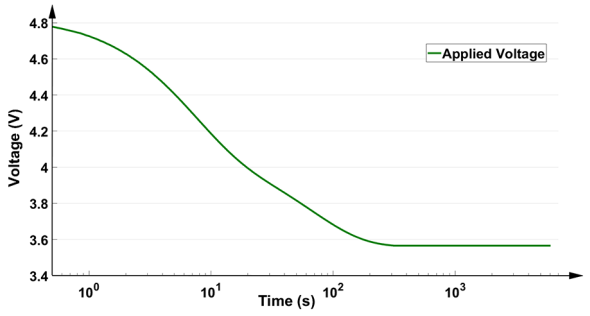


**Figure 7** The variation of applied voltage on the electrodes

point means $P_1(t) = P_2(t) = \cdots = P_n(t)$, which means the phase voltage $V^1_{\text{phase}} = V^2_{\text{phase}} = \cdots = V^n_{\text{phase}}$. Note that in practical experiments, the drift voltage varies continuously over time while the bias voltage is discretely applied by a power. The experimental result is shown in Fig. 6. We compared the output intensities of the modulator with and without multi-stable scheme within about thirty hours. It is obverse that the output intensity of the modulator drifts much less when the multi-stable scheme is applied, the drift magnitude with multi-step stable scheme is only 1.61 % of that without one.

The variation of the voltage applied on the electrodes is shown in Fig. 7, result shows that applied voltage on the tested modulator is monotonically decreasing. This is obvious, since the drift induced by the applied bias voltage is monotonous and leads to an increasing phase voltage, hence the applied voltage should be decreased in order to keep the working point stable. Furthermore, as shown in Fig. 4(b), the bias drift becomes less steep over time, thus the decline of applied bias voltage also slows down.

The result in Fig. 6 clearly shows that our multi-step stable scheme is efficient on the modulator. In addition, to verify whether the multi-step stable scheme is general to all the LNMZ based modulators, we tested the scheme on another LNMZ type intensity modulator. This modulator is manufactured by SUMITOMO OSAKA CEMENT, the extinction ratio is over 20 dB, driving voltage $V_\pi$ at 10 Gbps is 6.0 Vpp. The experimental result is presented in Fig. 8, it is clear that our stable scheme is also efficient on this modulator. Comparing the output intensities, the drift magnitude with multi-step stable scheme is only 5.03 % of that without one. This result shows that our multi-step scheme is general

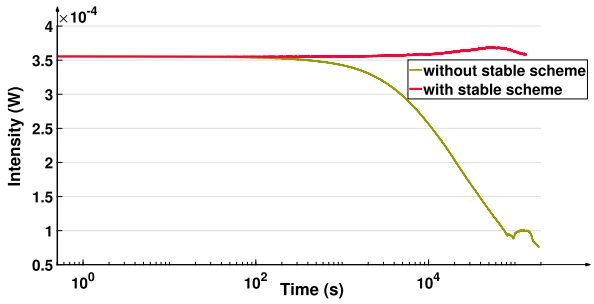


**Figure 8** Experimental multi-step test on another LNMZ type intensity modulator. The drift magnitude with multi-step stable scheme is only 5.03 % of that without one

to LNMZ based modulator, it make sense because RC circuit model describing the drift is based on the inhomogeneous electrical properties inside the modulator, and these properties is mainly resulted from the electrically anisotropic and the inhomogeneous electrical properties of $LiNbO_3$ layer, thus we believe the RC circuit model is general to describe the electrical charge relaxation inside LNMZ type modulators.

Experiments above indicates that the multi-step bias stable scheme is in fact a bias modulating strategy, it predicts the bias drift after multi-step bias voltage applied on the modulator instead of adding any feedback modules. Considering a QKD system, this scheme is superior to exiting bias control methods [27–32]. For the aspect of system performance, in exiting methods, both utilizing optical power monitor and dither signals will need external signal monitoring module, which will increase the complexity of QKD systems. However, our scheme is based on the RC circuit model, the bias drift is predicted by the model rather than using signal monitoring, the validity of our scheme comes from the validity of RC circuit model and many works have proofed that RC circuit model can accurately reveal the bias drift, so the prediction of model Eq. (6) is reliable, thus we can obtain a bias modulating strategy to keep the bias drift magnitude S(t) = 0, which means the bias drift of the modulator is 0, without any feedback modules in this process. This is important in QKD systems, especially in a high repeation rate system, the performance of the QKD system is limited by overall bandwidth, including the feedback module. Furthermore, QKD systems generate secret keys with quantum signals, a dither signal from exiting methods may induce noise and also affect the key rate performance of the systems. For the aspect of security, the dither signals may also cause photoinduced index change of the LNMZ based modulators, known as photorefractive effect. Reports show that photorefractive effect in $LiNbO_3$ can be utilized as a potential loophole to carry out malicious attacks by injecting an optimized irradiation beam with only several nanowatts [36, 37]. In QKD systems, this kind of side channel can not be neglected when dither signals are utilized to overcome the bias drift. However, our scheme in Eq. (6) can work without optical feedback modules or dither signals, thus it can be more reliable in the presence of this side channel.

## 4 The affect on the QKD system

In this section, we analyzed how the DC bias drift affect the key rate of QKD system. We presented a simulation on the twin-field QKD protocol (TF-QKD) [38]. TF-QKD is a novel protocol that is proved to overcoming the rate–distance limit of quantum key distribution. Many variants [39–46] of the original protocol have been proposed to further

**Table 1** The simulation parameters. $\eta$ is the detection efficiency of single photon detectors, $\eta_d$ is dark counting rate, $f$ is the correction efficiency, $e_d$ is the misalignment error probability

| $\eta$ | $\eta_d$ | Fiber loss | $f$ | $e_d$ |
|---|---|---|---|---|
| 30% | $10^{-7}$ | 0.2 dB/km | 1.1 | 0.02 |

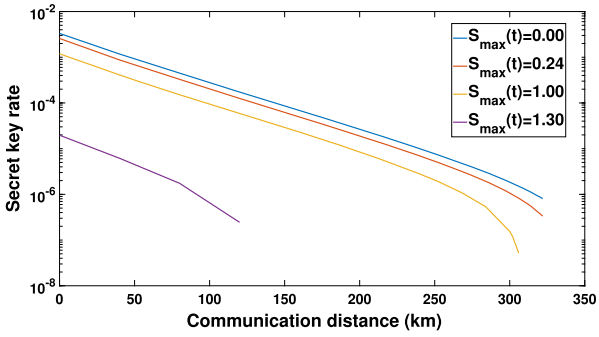


**Figure 9** The performance of TF-QKD with and without stable scheme

improve the security and performance of original protocol. Experimental demonstration of TF-QKD have been presented as well [12, 47–54]. Here we implemented simulation of a variant named sending-or-not-sending TF-QKD (SNS-TFQKD) [40, 55], and the simulation parameters in our simulation are listed in Table 1. For simplicity, our simulation result is calculated without AOPP method [56, 57], this is feasible when we just care about the key rate drop caused by bias drift. The result is presented in Fig. 9, here we compare the key rates with three different maximum bias drift magnitude 0.00, 0.24 and 1.00, where 0.24 is the maximum bias drift magnitude $S(t)$ of the first modulator we tested, and $S(t)$ of the second modulator can reach 1.00. The result shows that the bias drift affects the key rate of QKD system. Furthermore, we also present the simulation where the drift magnitude is 1.30. When the drift magnitude reaches 1.30 the keys rates decline most, and the QKD system is nearly broken. This result verified the advantage of our method on bias control. However, one should note that here are no modulator can work perfectly, a small offset voltage drift will still lead to intensity fluctuation. There are still works to do to further eliminate the affect of intensity fluctuation, Ref. [58] proposed a strict method for calculating the key rate of the SNS-TFQKD protocol with source errors. They obtained the key rate formulas under the premise of ensuring the protocol's security. Additionally, the SNS-TFQKD protocol's farthest distance slightly decreases as the intensity fluctuation range increases, indicating that the SNS-TFQKD protocol is robust against source errors.

In conclusion, we have demonstrated a RC circuit model to describe the DC bias drift in the LNMZ intensity modulator. The RC model is verified at different working point. Furthermore, we proposed a multi-step stable scheme. In the scheme, we adjust the given bias voltage continuously according to Eq. (6), aiming to keep the output intensity stable. Result shows that our scheme can eliminate the bias drift within a range of thirty hours. In fact, our scheme is based on the RC circuit model, and the RC circuit model is efficient to reveal the electrical evolution inside the modulator within a long time range, to some extent, as long as we need. Thus we believe our multi-step scheme can have a good performance at a time range more than thirty hours. Besides, from Eq. (6) we can know the

multi-step scheme is essentially a voltage strategy guiding how to apply the bias, we do not have to monitor the output intensity, so there is no need of any feedback mechanisms. To this end, the multi-step scheme will not increase the experimental complexity and is more suitable for a QKD system. What is more, the $P_n(t)$ in Eq. (6) is the model of predicting drift magnitude at time $t$, to maintain the bias working point means $P_1(t) = P_2(t) = \cdots = P_n(t)$. Interestingly, if we modify the relation of $P_n(t)$, $n = 1, 2, 3, \ldots$, the model in Eq. (6) can be competent for other tasks. This means we can control the bias working point at different circumstance more than maintain it. We also presented simulations to study how DC bias drift affect the QKD system. Simulation result shows the key rates drop quickly as the drift magnitude $S(t)$ increase, and the QKD system is nearly broken when $S(t)$ researches 1.30.

## Appendix: Analysis of the internal and external factors

In this section, we analyze and compare the external and internal factors that lead to the bias drift in a LNMZ modulator. External factors are linked to the change of effective refractive index of the waveguide via the variations of external environment, mainly including temperature, optical power and the mechanical stress, which are related to thermo-optic, pyroelectric effect, photorefractive effect and strain-optic effect respectively. Many researches on external factors have been implemented so far [26, 59–63]. It is believed that extrinsic physical effects induce bias drift on the LNMZ modulator when the waveguides are unbalanced or the external excitation is unsymmetrical. Ref. [26] calculated the drift magnitude $S$ for unbalanced modulator (length difference between the two arms is $\delta = 1.3$ μm) with symmetrical excitation, the results show that thermal drift is 6%, photo-induced drift is $10^{-5}$% and strain optical drift is $4 \times 10^{-2}$%, this indicates that thermal drift is predominant in extrinsic sources of bias drift.

The thermal drift originates from both thermo-optic and pyroelectric properties. The thermo-optic effect gives rise to a change of the effective refractive index of the material. In contrary, since $LiNbO_3$ crystal is pyroelectric, the pyroelectric effect induces transient contribution to the drift, making thermal drift a complex process. A Sellmeier equation is used to predict the refractive index for $n_e$ in $LiNbO_3$ [25].

Nevertheless, reports have shown that extrinsic drift amplitudes are of weak importance when compared to the overall drift magnitude reported in the literature that can reach over 100% [26]. We also made a simple test about the working point drift resulting from temperature variation. In our test, the bias voltage applied on the modulator is set to 0 V to eliminate the influence of bias voltage, the temperature in the chamber is varied from 20°C to 30°C, which is the usual temperature range in the lab environment, we record the output optical power of the modulator and the power drift is converted into the change of phase voltage, we compared the phase voltage drift from temperature and bias voltage corresponds to quadrature working point. Results are shown in Fig. 10, the drift from quadrature voltage and temperature variations are 1.4552 V and 0.0353 V respectively, it shows the temperature drift is two magnitudes smaller than quadrature drift. This indicates thermal drift is negligible compared to the quadrature drift in the lab environment, confirming that bias voltage is the dominant reason for bias drift of LNMZ modulators. Note that in our experiments, we mainly care about the electrical inhomogeneous inside the LNMZ modulator, thus the modulator is placed in a temperature-controlled chamber within 0.01 degree to eliminate the bias drift induced by thermo drift, we think it will not significantly reduce the effectiveness of our bias stable scheme even without the temperature controller. Our goal is to verify the universality of our simplified RC circuit model, we only change the applied bias voltage and try to keep other extrinsic factors unchanged, including temperature and stress.

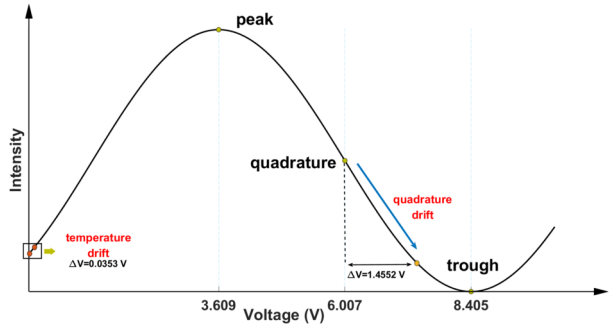


**Figure 10** Comparison of the working point drift induced from bias voltage and temperature variation

**Acknowledgements**
The authors thank the CAS Key Laboratory of Quantum Information, the CAS Center for Excellence in Quantum Information and Quantum Physics and the Hefei National Laboratory.

**Funding**
This work has been supported by the National Natural Science Foundation of China (No. 62271463, 62171424, and 62105318), the China Postdoctoral Science Foundation (2022M723064,2021M693098); and the Anhui Initiative in Quantum Information Technologies.

**Availability of data and materials**
The data that support the findings of this study are available from the corresponding author upon reasonable request.

## Declarations

**Ethics approval and consent to participate**
Not applicable.

**Competing interests**
The authors declare no competing interests.

**Author contributions**
JT start the project and design the experiment. JT, SW, and D-YH perform the experiment and complete the data analysis. G-JF-Y, provide the theoretical calculations. Z-QY, WC, G-CG and Z-FH supervise the project. All authors read and approved the final manuscript.

**Author details**
[1]CAS Key Laboratory of Quantum Information, University of Science and Technology of China, Hefei 230026, P.R. China. [2]CAS Center for Excellence in Quantum Information and Quantum Physics, University of Science and Technology of China, Hefei 230026, P.R. China. [3]Hefei National Laboratory, University of Science and Technology of China, Hefei 230088, P.R. China.

Received: 23 March 2023 Accepted: 15 August 2023 Published online: 07 September 2023

**References**

1. Bennett CH, Brassard G. Proceedings of the IEEE international conference on computers, systems and signal processing. 1984.
2. Ekert AK. Quantum cryptography based on bell's theorem. Phys Rev Lett. 1991;67:661.
3. Lo H-K, Chau HF. Unconditional security of quantum key distribution over arbitrarily long distances. Science. 1999;283:2050.
4. Inoue K, Waks E, Yamamoto Y. Differential phase shift quantum key distribution. Phys Rev Lett. 2002;89:037902.
5. Gobby C, Yuan ZL, Shields AJ. Quantum key distribution over 122 km of standard telecom fiber. Appl Phys Lett. 2004;84:3762.
6. Zhao Y, Qi B, Ma X, Lo H-K, Qian L. Experimental quantum key distribution with decoy states. Phys Rev Lett. 2006;96:070502.
7. Lo H-K, Curty M, Qi B. Measurement-device-independent quantum key distribution. Phys Rev Lett. 2012;108:130503.
8. Wang C, Song X-T, Yin Z-Q, Wang S, Chen W, Zhang C-M, Guo G-C, Han Z-F. Phase-reference-free experiment of measurement-device-independent quantum key distribution. Phys Rev Lett. 2015;115:160502.
9. Zhou Y-H, Yu Z-W, Wang X-B. Making the decoy-state measurement-device-independent quantum key distribution practically useful. Phys Rev A. 2016;93:042324.
10. Yin H-L, Chen T-Y, Yu Z-W, Liu H, You L-X, Zhou Y-H, Chen S-J, Mao Y, Huang M-Q, Zhang W-J et al. Measurement-device-independent quantum key distribution over a 404 km optical fiber. Phys Rev Lett. 2016;117:190501.
11. Liao S-K, Cai W-Q, Liu W-Y, Zhang L, Li Y, Ren J-G, Yin J, Shen Q, Cao Y, Li Z-P et al. Satellite-to-ground quantum key distribution. Nature. 2017;549:43.
12. Wang S et al. Twin-field quantum key distribution over 830-km fibre. Nat Photonics. 2022;16(2):154–61.
13. Fan-Yuan G-J, Lu F-Y, Wang S, Yin Z-Q, He D-Y, Zhou Z, Teng J, Chen W, Guo G-C, Han Z-F. Measurement-device-independent quantum key distribution for nonstandalone networks. Photon Res. 2021;9:1881.
14. Fan-Yuan G-J, Lu F-Y, Wang S, Yin Z-Q, He D-Y, Chen W, Zhou Z, Wang Z-H, Teng J, Guo G-C et al. Robust and adaptable quantum key distribution network without trusted nodes. Optica. 2022;9:812.
15. Hwang W-Y. Quantum key distribution with high loss: toward global secure communication. Phys Rev Lett. 2003;91:057901.
16. Lo H-K, Ma X, Chen K. Decoy state quantum key distribution. Phys Rev Lett. 2005;94:230504.
17. Wang X-B. Beating the photon-number-splitting attack in practical quantum cryptography. Phys Rev Lett. 2005;94:230503.
18. Li G, Yu P. Optical intensity modulators for digital and analog applications. J Lightwave Technol. 2003;21:2010.
19. Wooten EL, Kissa KM, Yi-Yan A, Murphy EJ, Lafaw DA, Hallemeier PF, Maack D, Attanasio DV, Fritz DJ, McBrien GJ et al. A review of lithium niobate modulators for fiber-optic communications systems. IEEE J Sel Top Quantum Electron. 2000;6:69.
20. Fu Y, Zhang X, Hraimel B, Liu T, Shen D. Mach-Zehnder: a review of bias control techniques for Mach-Zehnder modulators in photonic analog links. IEEE Microw Mag. 2013;14:102.

21. Li Y, Zhang Y, Huang Y. Any bias point control technique for Mach–Zehnder modulator. IEEE Photonics Technol Lett. 2013;25:2412.
22. Nagata H, Kiuchi K. Temperature dependence of dc drift of Ti: $LiNbO_3$ optical modulators with sputter deposited $SiO_2$ buffer layer. J Appl Phys. 1993;73:4162.
23. Nagata H, O'Brien N, Bosenberg W, Reiff G, Voisine K. Dc-voltage-induced thermal shift of bias point in $LiNbO_3$ optical modulators. IEEE Photonics Technol Lett. 2004;16:2460.
24. Nagata H, Kiuchi K, Saito T. Studies of thermal drift as a source of output instabilities in Ti: $LiNbO_3$ optical modulators. J Appl Phys. 1994;75:4762.
25. Jundt DH. Temperature-dependent Sellmeier equation for the index of refraction, n e, in congruent lithium niobate. Opt Lett. 1997;22:1553.
26. Salvestrini JP, Guilbert L, Fontana M, Abarkan M, Gille S. Analysis and control of the DC drift in $LiNbO_3$ based Mach–Zehnder modulators. J Lightwave Technol. 2011;29:1522.
27. Zhu X, Zheng Z, Zhang C, Zhu L, Tao Z, Chen Z. Coherent detection-based automatic bias control of Mach–Zehnder modulators for various modulation formats. J Lightwave Technol. 2014;32:2502.
28. Kim M-H, Yu B-M, Choi W-Y. A Mach-Zehnder modulator bias controller based on OMA and average power monitoring. IEEE Photonics Technol Lett. 2017;29:2043.
29. Yuan X, Zhang J, Zhang M et al. Any point bias control technique for MZ modulator. Optik. 2019;178:918.
30. Wang LL, Kowalcyzk T. A versatile bias control technique for any-point locking in lithium niobate Mach–Zehnder modulators. J Lightwave Technol. 2010;28:1703.
31. Gui T, Li C, Yang Q, Xiao X, Meng L, Li C, Yi X, Jin C, Li Z. Auto bias control technique for optical OFDM transmitter with bias dithering. Opt Express. 2013;21:5833.
32. Zhu M, Zhang H, Li L. Low noise arbitrary bias point control technique of IQ Mach-Zehnder modulator. Asia Communications and Photonics Conference. Optica Publishing Group, 2009.
33. Yamada S, Minakata M. DC drift phenomena in $LiNbO_3$ optical waveguide devices. Jpn J Appl Phys. 1981;20:733.
34. Becker RA. Circuit effect in $LiNbO_3$ channel-waveguide modulators. Opt Lett. 1985;10:417.
35. Korotky S, Veselka J. An RC network analysis of long term Ti: $LiNbO_3$ bias stability, lightwave technology. J Lightwave Technol. 1996;14:2687.
36. Ye P, Chen W, Zhang G-W, Lu F-Y, Wang F-X, Huang G-Z, Wang S, He D-Y, Yin Z-Q, Guo G-C et al. Induced-photorefraction attack against quantum key distribution. Phys Rev Appl. 2023;19:054052.
37. Lu F-Y, Ye P, Wang Z-H, Wang S, Yin Z-Q, Wang R, Huang X-J, Chen W, He D-Y, Fan-Yuan G-J et al. Hacking measurement-device-independent quantum key distribution. Optica. 2023;10:520.
38. Lucamarini M, Yuan ZL, Dynes JF, Shields AJ. Overcoming the rate–distance limit of quantum key distribution without quantum repeaters. Nature. 2018;557:400.
39. Ma X, Zeng P, Zhou H. Phase-matching quantum key distribution. Phys Rev X. 2018;8:031043.
40. Wang X-B, Yu Z-W, Hu X-L. Twin-field quantum key distribution with large misalignment error. Phys Rev A. 2018;98:062323.
41. Cui C, Yin Z-Q, Wang R, Chen W, Wang S, Guo G-C, Han Z-F. Twin-field quantum key distribution without phase postselection. Phys Rev Appl. 2019;11:034053.
42. Curty M, Azuma K, Lo H-K. Simple security proof of twin-field type quantum key distribution protocol. npj Quantum Inf. 2019;5:64.
43. Lin J, Lütkenhaus N. Simple security analysis of phase-matching measurement-device-independent quantum key distribution. Phys Rev A. 2018;98:042332.
44. Zhou X-Y, Zhang C-H, Zhang C-M, Wang Q. Asymmetric sending or not sending twin-field quantum key distribution in practice. Phys Rev A. 2019;99:062316.
45. Zhang C-H, Zhang C-M, Wang Q. Twin-field quantum key distribution with modified coherent states. Opt Lett. 2019;44:1468.
46. Wang R, Yin Z-Q, Lu F-Y, Wang S, Chen W, Zhang C-M, Huang W, Xu B-J, Guo G-C, Han Z-F. Optimized protocol for twin-field quantum key distribution. Commun Phys. 2020;3:149.
47. Wang S, He D-Y, Yin Z-Q, Lu F-Y, Cui C-H, Chen W, Zhou Z, Guo G-C, Han Z-F. Beating the fundamental rate-distance limit in a proof-of-principle quantum key distribution system. Phys Rev X. 2019;9:021046.
48. Minder M, Pittaluga M, Roberts G, Lucamarini M, Dynes J, Yuan Z, Shields A. Experimental quantum key distribution beyond the repeaterless secret key capacity. Nat Photonics. 2019;13:334.
49. Liu Y, Yu Z-W, Zhang W, Guan J-Y, Chen J-P, Zhang C, Hu X-L, Li H, Jiang C, Lin J et al. Experimental twin-field quantum key distribution through sending or not sending. Phys Rev Lett. 2019;123:100505.
50. Zhong X, Hu J, Curty M, Qian L, Lo H-K. Proof-of-principle experimental demonstration of twin-field type quantum key distribution. Phys Rev Lett. 2019;123:100506.
51. Chen J-P, Zhang C, Liu Y, Jiang C, Zhang W, Hu X-L, Guan J-Y, Yu Z-W, Xu H, Lin J et al. Sending-or-not-sending with independent lasers: secure twin-field quantum key distribution over 509 km. Phys Rev Lett. 2020;124:070501.
52. Pittaluga M et al. 600-km repeater-like quantum communications with dual-band stabilization. Nat Photonics. 2021;15(7):530–5.
53. Liu H, Jiang C, Zhu H-T, Zou M, Yu Z-W, Hu X-L, Xu H, Ma S, Han Z, Chen J-P et al. Field test of twin-field quantum key distribution through sending-or-not-sending over 428 km. Phys Rev Lett. 2021;126:250502.
54. Chen J-P et al. Twin-field quantum key distribution over a 511 km optical fibre linking two distant metropolitan areas. Nat Photonics. 2021;15(8):570–5.
55. Yu Z-W, Hu X-L, Jiang C, Xu H, Wang X-B. Sending-or-not-sending twin-field quantum key distribution in practice. Sci Rep. 2019;9:3080.
56. Xu H, Yu Z-W, Jiang C, Hu X-L, Wang X-B. Sending-or-not-sending twin-field quantum key distribution: breaking the direct transmission key rate. Phys Rev A. 2020;101:042330.
57. Jiang C, Hu X-L, Yu Z-W, Wang X-B. Composable security for practical quantum key distribution with two way classical communication. New J Phys. 2021;23:063038.
58. Jiang C, Yu Z-W, Hu X-L, Wang X-B. Robust twin-field quantum key distribution through sending or not sending. Nat Sci Rev. 2023;10:nwac186.

59. Nagata H, Ichikawa J. Progress and problems in reliability of Ti: $LiNbO_3$ optical intensity modulators. Opt Eng. 1995;34:3284.
60. Seino M et al. A low dc-drift Ti: $LiNbO_3$ modulator assured over 15 years. Optical Fiber Communication Conference. Optica Publishing Group, 1992.
61. Schmidt R, Cross P, Glass A. Optically induced crosstalk in $LiNbO_3$ waveguide switches. J Appl Phys. 1980;51:90.
62. Betts G, O'Donnell F, Ray K. Effect of annealing on photorefractive damage in titanium-indiffused $LiNbO_3$ modulators. IEEE Photonics Technol Lett. 1994;6:211.
63. Nagata H, Kiuchi K, Sugamata T. Refractive index fluctuations in deformed Ti: $LiNbO_3$ waveguides due to $SiO_2$ overlayer deposition. Appl Phys Lett. 1993;63:1176.

## Publisher's Note